JOURNAL OF GEOPHYSICAL RESEARCH: OCEANS, VOL. 118, 5977–5993, doi:10.1002/2013JC008924, 2013

A comparison of mechanisms generating vertical transport in the Brazilian coastal upwelling regions

P. L. F. Mazzini[1] and J. A. Barth[1]

Received 13 March 2013; revised 13 September 2013; accepted 7 October 2013; published 13 November 2013.

[1] Several mechanisms can drive vertical velocities in the coastal ocean, including wind-forcing and through gradients in the vorticity field generated by flow-topography interactions. A two-layer, steady, wind-driven, analytical model is applied to the major upwelling systems of Brazil: Cabo Frio (CF) and Cabo de Santa Marta (CSM) regions. Comparisons are made between the relative roles of wind and flow-topography interaction in inducing upwelling over these regions. Ekman pumping is the weakest mechanism over the shelf, but does influence the along-shelf temperature in the CF area. Away from coastline irregularities, wind-driven upwelling (Ekman transport) dominates over all mechanisms. However, in the vicinity of capes and coastal features, topographically driven upwelling plays a significant role, and its transports may vary from 43% to 94% of wind-driven upwelling. Upstream of capes, topographically driven vertical motions are downwelling favorable and act against the wind-driven coastal upwelling, while downstream of capes, they are upwelling favorable, where all mechanisms add up to create strong upwelling. Peaks in total upwelling in the CF region are about twice as large as those in the CSM area because the CF region has stronger winds and larger coastline perturbations than in the CSM region. Observed sea surface temperatures (SST) agree well with variability in the vertical transports where upwelling peaks are in phase with low temperature peaks along the coast. Results suggest that on larger scales, the SST variability along the coast is mainly controlled by wind-driven upwelling, while upwelling due to flow-topography interaction is responsible for the smaller scale SST variability.

Citation: Mazzini, P. L. F., and J. A. Barth (2013), A comparison of mechanisms generating vertical transport in the Brazilian coastal upwelling regions, *J. Geophys. Res. Oceans*, *118*, 5977–5993, doi:10.1002/2013JC008924.

1. Introduction

[2] When wind blows over the continental shelves, moving with the coast on its right (left) in the southern hemisphere (northern hemisphere), water is directed offshore by surface Ekman transport [*Ekman*, 2000]. The presence of the coast, acting as a natural barrier, creates a divergence of the flux, and due to conservation of mass, upward vertical velocities are produced, commonly referred to as "coastal upwelling."

[3] Upwelling is an important mechanism for carrying cold, dense, nutrient-rich waters into the euphotic zone, therefore having a significant impact on regional climate and marine ecosystems. Upwelling also creates horizontal temperature and density gradients near the surface, which drives strong geostrophic alongshore currents, and influences the exchange of heat and gases between the ocean and atmosphere.

[4] On the south and southeast Brazilian shelves (Figure 1), persistent upwelling-favorable winds are present throughout the year north of Rio de Janeiro (22.9°S, 43.2°W) (limited by approximately 19.5°S and 17.5°S during Fall and Winter, respectively) and are present during spring and summer south of Ilha de Santa Catarina (27.6°S, 48.5°W). The large-scale, quasi-steady feature in the atmosphere responsible for this scenario is the South Atlantic High Pressure system. Significant perturbations on the wind field over the region commonly occur due to the passage of synoptic weather systems, traveling from southwest toward northeast, and getting weaker as they reach lower latitudes. Perturbations are more energetic during the fall and particularly in the wintertime, when they can reverse the wind field and cause the upwelling to shutdown [*Stech and Lorenzzetti*, 1987]. These perturbations affect the climatological mean wind stress and result in a very low mean wind stress during fall, and winter, especially in the southern regions, where the systems are more energetic (Figure 1).

[5] Cross-shelf sea surface temperature (SST) gradients are coherent with the wind stress directions according to

[1]College of Earth, Ocean, and Atmospheric Sciences, Oregon State University, Corvallis, Oregon, USA.

Corresponding author: P. L. F. Mazzini, College of Earth, Ocean, and Atmospheric Sciences, Oregon State University, 104 CEOAS Administration Bldg., Corvallis, OR 97331-5503, USA. (pmazzini@coas.oregonstate.edu)

2169-9275/13/10.1002/2013JC008924

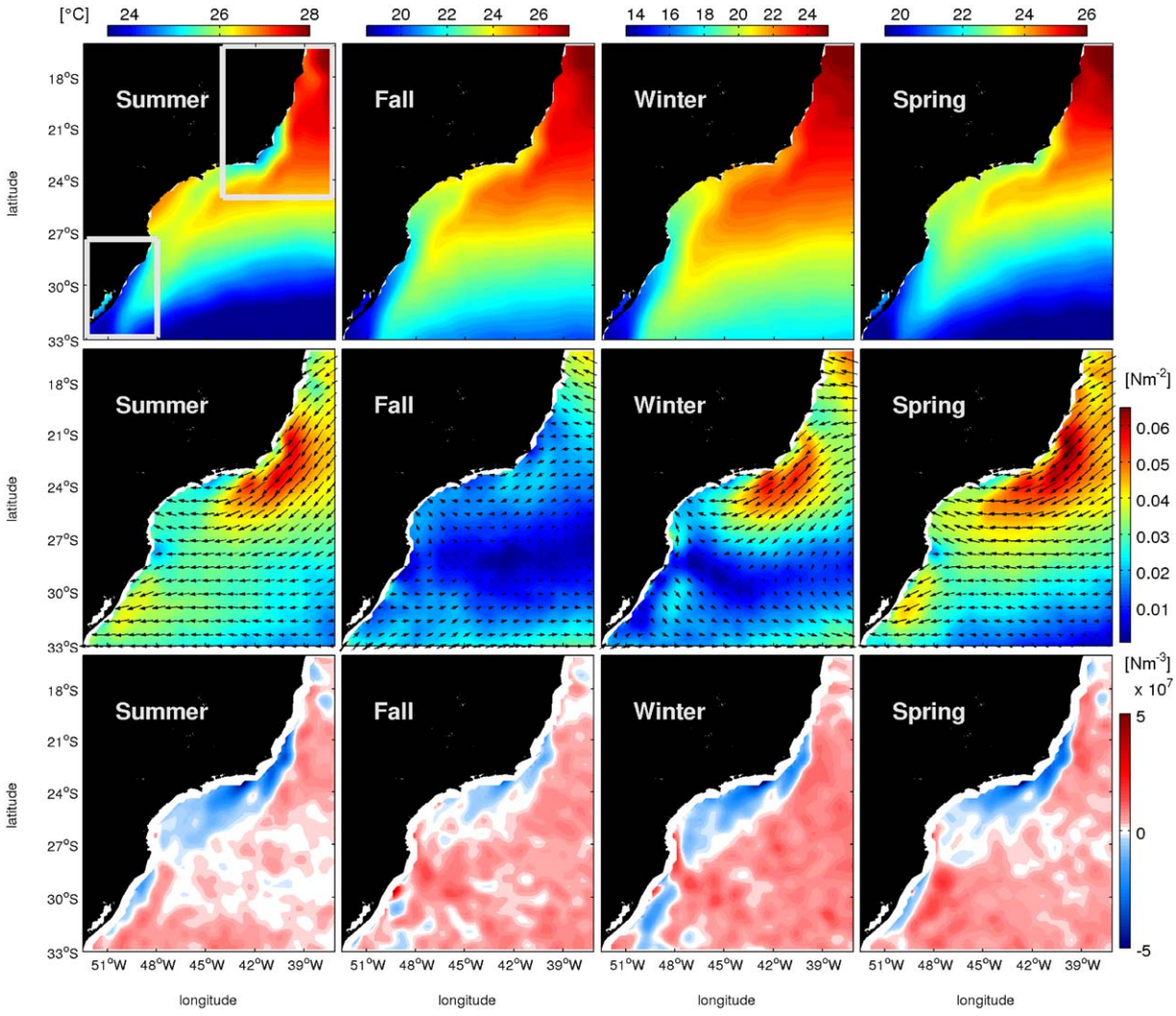

Figure 1. Seasonal climatologies of sea surface temperature (SST) from the (top) Advanced Very High Resolution Radiometer (NOAA AVHRR v2.), (middle) wind stress, and (bottom) wind stress curl from the SeaWinds Scatterometer on the QuikSCAT satellite data [*Risien and Chelton*, 2001]. White boxes indicate regions where vertical velocities are calculated.

"coastal upwelling" theory for those regions (Figure 1), with the exception of Fall and Winter south of Cabo de Santa Marta (CSM), when the cold waters along the southern coast are not driven by upwelling, but instead are advected from the Argentinian and Uruguayan shelves by the northward currents often occurring during these seasons [*Pereira*, 2000; *Campos et al*., 1996; *Lima et al*., 1979; *Campos et al*., 1999; *Piola et al*., 2005; *Lentini et al*., 1996; *Soares and Möller*, 2004; *Zavialov et al*., 2002; *Souza and Robinson*, 2007; *Piola et al*., 2008, 2008; *Campos et al*., 2013]. Several studies presented observational evidence of the coastal upwelling phenomenon occurring at Cabo Frio (CF) [*Allard*, 1955; *Emílsson*, 1905; *Ikeda et al*., 1980; *Magliocca et al*., 2010; *Castro and Miranda*, 1998; *Rodrigues and Lorenzzetti*, 2001] and south of Cabo de Santa Marta [*Lima et al*., 1979; *Möller et al*., 2009; *Campos et al*., 2013].

[6] A second mechanism by which the wind can induce vertical velocities, without the need for the coastal boundary, is by having a horizontally nonhomogeneous wind field (nonzero wind stress curl), which creates a divergence of the Ekman transport within the Ekman layer, and—again, by continuity, upwelling/downwelling takes place. This is called Ekman pumping.

[7] *Castelão and Barth* [2006b] used wind stress data derived from the Sea Winds scatterometer from the QuikSCAT satellite to study the contribution of Ekman pumping to the upwelling system around Cabo Frio. The authors integrated Ekman pumping velocities up to approximately 200 km off the coast, where the upwelling favorable negative wind stress curl is seen (Figure 1), and showed that this mechanism is as important as the coastal upwelling for the total vertical transport of the region, and that it also contributes to the spatial dependence of the upwelling and SST distribution along the coast.

[8] *Campos et al*. [2013] estimated Ekman pumping transport at Cabo de Santa Marta region using two different wind products, from QuikSCAT satellite and from Blended Sea Winds climatology (http://www.ncdc.noaa.gov/oa/rsad/air-sea/seawinds.html), and integrating Ekman pumping velocities up to nearly 100 km offshore (where negative

wind stress curl is observed). As a contrast to Cabo Frio region, the authors found that this mechanism does not seem to play a significant role in generating upwelling events off Cabo de Santa Marta.

[9] The intensification of upwelling around capes has been observed in many different regions around the world, and often it is possible to see events occurring around the regions of Cabo Frio and Cabo de Santa Marta using sea surface temperature (SST) satellite images. *Arthur* [1965] approached this problem through the use of vorticity conservation principles and elucidates how coastline irregularities that can cause the currents to change curvature, and also produce along-shelf variations in the cross-shelf horizontal shear, can generate upwelling. These two mechanisms will be discussed in more detail in the next section.

[10] The role of bottom topography and coastline geometry on upwelling in the Cabo Frio region was studied by *Rodrigues and Lorenzzetti* [2001]. The authors used a two-layer finite element model forced by constant wind stress simulating three distinct scenarios: (1) a real bottom topography and a real coastline; (2) a flat-bottom topography and a real coastline; and (3) a real bottom topography and a smoothed coastline. They concluded that the local bottom topography and coastline geometry affect the upwelling magnitude in the entire domain, and that coastline irregularities dominate over bottom topographic variations in determining the location of Cabo Frio upwelling.

[11] *Campos et al*. [2013] used a full nonlinear primitive equation numerical model to investigate the role of bathymetric variations on the upwelling of Cabo de Santa Marta. The authors proposed that during northeasterly winds an intensification of a southward current occur, and in conjunction with a middle-shelf flow divergence promoted by the shelf expansion, an inshore flow is driven near the bottom that can enhance the upwelling south of the cape.

[12] As described above, considerable effort has been made to understand upwelling phenomena in the Cabo Frio and Cabo de Santa Marta regions, however, a direct comparison of the transport magnitudes driven by wind-forced upwelling mechanisms and flow-topography interaction has not yet been done.

[13] The goal of this paper is to estimate and compare vertical transports induced by four mechanisms: Ekman transport ("coastal upwelling"), Ekman pumping, horizontal shear due to coastline irregularities and coastline curvature, for the regions of Cabo Frio and Cabo de Santa Marta, Brazil. In order to do these calculations, we use wind stress data from the QuikSCAT satellite [*Risien and Chelton*, 2001] and an analytical, two-layer, steady, wind-driven model [*Johnson et al*., 2001] used by *Figueroa and Moffat* [1998] to study the upwelling system of Chile, which included three mechanisms: Ekman transport, Ekman pumping, and horizontal shear due to coastline irregularities. Since upwelling due to curved flow around capes may be important in the Brazilian upwelling region, we include this mechanism which was previously omitted by *Figueroa and Moffat* [1998].

2. Two-Layer Upwelling Model

[14] An extension of *Arthur*'s [1965] vorticity analysis to include the effects of stratification and wind-forcing was done by *Johnson et al*. [2001]. The authors derived a two-layer, steady, analytical model forced by alongshore wind stress. By allowing a cross-shelf component of wind stress forcing, the set of equations for the problem becomes:

$$u_1\frac{\partial u_1}{\partial x}+v_1\frac{\partial u_1}{\partial y}-fv_1=-\frac{1}{\rho_1}\frac{\partial p_1}{\partial x}+\frac{\tau_o^x}{\rho_1 h_1}, \tag{1}$$

$$u_1\frac{\partial v_1}{\partial x}+v_1\frac{\partial v_1}{\partial y}+fu_1=-\frac{1}{\rho_1}\frac{\partial p_1}{\partial y}+\frac{\tau_o^y}{\rho_1 h_1}, \tag{2}$$

$$w_{-h}=h_1\left(\frac{\partial u_1}{\partial x}+\frac{\partial v_1}{\partial y}\right), \tag{3}$$

$$u_2\frac{\partial u_2}{\partial x}+v_2\frac{\partial u_2}{\partial y}-fv_2=-\frac{1}{\rho_2}\frac{\partial p_2}{\partial x}, \tag{4}$$

$$u_2\frac{\partial v_2}{\partial x}+v_2\frac{\partial v_2}{\partial y}+fu_2=-\frac{1}{\rho_2}\frac{\partial p_2}{\partial y}, \tag{5}$$

$$w_{-h}=-h_2\left(\frac{\partial u_2}{\partial x}+\frac{\partial v_2}{\partial y}\right), \tag{6}$$

$$H=h_1+h_2, \tag{7}$$

where x is the cross-shelf direction, y the along-shelf direction, and z is the vertical direction. Subscripts 1 and 2 refer to upper and lower layer, respectively. The components of velocity in the x and y directions are denoted by u and v respectively, w_{-h} is the vertical velocity at the interface between the layers, h is the layer thickness, H is the total water depth, ρ is the water density, p is the pressure, τ_o^x is the component of wind stress perpendicular to the coast, τ_o^y is the component of wind stress parallel to the coast, and f is the Coriolis parameter.

[15] By cross-differentiating the x- and y-momentum equations, the authors eliminated the pressure gradient terms and obtained a vorticity equation for each layer:

$$w_{-h}=-\frac{h_1}{f}\left(\vec{V}_1\cdot\nabla\xi_1+\beta v_1\right)+\frac{h_1}{f}\left[\frac{\partial}{\partial x}\left(\frac{\tau_o^y}{\rho_1 h_1}\right)-\frac{\partial}{\partial y}\left(\frac{\tau_o^x}{\rho_1 h_1}\right)\right], \tag{8}$$

$$w_{-h}=\frac{h_2}{f}\left(\vec{V}_2\cdot\nabla\xi_2+\beta v_2\right), \tag{9}$$

where $\vec{V}$ is the velocity vector $\left(\vec{V}\equiv u\hat{i}+v\hat{j}\right)$, ξ is the vertical component of relative vorticity $\left(\xi\equiv\frac{\partial v}{\partial x}-\frac{\partial u}{\partial y}\right)$, β is the planetary vorticity gradient, and it is assumed that $\xi\ll f$.

[16] Now, the key assumption for the model is that *Johnson et al*. [2001] assumed that the layers have along-shelf velocities of the same magnitude, but opposite directions:

$$v_2=-v_1, \tag{10}$$

$$\vec{V}_2\cdot\nabla\xi_2=-\vec{V}_1\cdot\nabla\xi_1. \tag{11}$$

[17] It is then possible to combine equations (8) and (9), and get only one equation for the velocity at the interface between the two layers:

$$w_{-h} = -\frac{H}{2f}\left(\vec{V}_1 \cdot \nabla\xi_1 + \beta v_1\right) + \frac{h_1}{2f}\left[\frac{\partial}{\partial x}\left(\frac{\tau_o^y}{\rho_1 h_1}\right) - \frac{\partial}{\partial y}\left(\frac{\tau_o^x}{\rho_1 h_1}\right)\right]. \tag{12}$$

[18] The assumptions made in equations (10) and (11) have the advantage of reducing the problem to only one equation. Equation (12) allows us to estimate w_{-h} from knowing the upper layer horizontal velocity field, the wind-forcing and the upper layer thickness.

[19] Defining that the velocities of upper and lower layer are equal and opposite comes from the result of using a two-layer model instead of a $1\frac{1}{2}$-layer model. For the two-layer model, the lower layer is active and has finite depth, which is appropriate for an application in the coastal ocean. So changes in the interface height in this case, will change upper and lower layer vorticity, and hence velocity, therefore the system is coupled. This is consistent with other examples of two-layer models used in studying continental shelf dynamics [e.g., *Allen*, 1975, 1976; *Crépon and Richez*, 1984; *Crépon et al*., 1961].

[20] Three different mechanisms besides coastal upwelling that can drive vertical velocities in the ocean are apparent in equation (12): advection of relative vorticity gradients, advection of planetary vorticity gradients (via the Sverdrup vorticity balance), and wind stress curl. The way that coastline/topography can induce upwelling becomes clear by looking at the definition of relative vorticity (ξ) in natural coordinates:

$$\xi = -\frac{\partial V}{\partial n} + \frac{V}{R}, \tag{13}$$

where V is the current speed, n is the normal direction to the streamlines, and R is the radius of curvature of a streamline.

[21] The cross-shelf horizontal shear of currents will generate vorticity by the first term in the right-hand side of equation (13) and the coastline curvature can cause the currents to turn, generating vorticity by the second term in the right-hand side of equation (13). Now, coastline irregularities will cause the currents to change curvature and change horizontal shear, creating spatial gradients of relative vorticity along the coast, which will induce vertical velocities by the first term in the right hand side of equation (12).

[22] *Figueroa and Moffat* [1998] used *Johnson et al*.'s [1980] model (equation (12)) with a few modifications to investigate the contribution from different terms in the total upwelling of the Chilean coast: "coastal upwelling," Ekman pumping and vertical velocities induced by changes of horizontal shear due to topographic effects. Vertical velocities driven by advection of planetary vorticity gradients were not included by *Figueroa and Moffat* [1998] because they have an insignificant contribution to the total upwelling for the spatial scale of interest, as previously shown by *Arthur* [1965] through scaling analysis.

[23] Vertical velocities from coastal upwelling ($w_{coastal}$) are added to the model and calculated by:

$$w_{coastal} = \frac{\tau_o^y}{\rho_1 f \lambda_i}, \tag{14}$$

where τ_o^y is the wind stress component parallel to the coast, and λ_i is the cross-shore length scale of the upwelling, typically the internal Rossby radius of deformation, and it is assumed that vertical velocities induced by coastal upwelling are zero beyond λ_i.

[24] Ekman pumping (w_{curl}) driven vertical velocities from equation (12), with the additional assumption that cross-shelf variations in h_1 are small, consistent with linear two-layer upwelling model, becomes:

$$w_{curl} = \frac{1}{2\rho_1 f}\left(\frac{\partial \tau_o^y}{\partial x} - \frac{\partial \tau_o^x}{\partial y}\right). \tag{15}$$

[25] For the vertical velocities induced by changes of horizontal shear due to topographic effects (w_{tshear}), *Figueroa and Moffat* [1998] assumed a steady upwelling jet, in water of depth H, and with a linear horizontal velocity profile (constant horizontal shear) from zero at the coast to a maximum at a distance S, which in this case the relative vorticity can be simplified to $\xi = \frac{\partial v}{\partial x}$. With the additional assumption that the offshore boundary of the jet remains straight and at a fixed distance from the mean shoreline, then changes in coastline orientation will only change the along-shelf velocities of the jet, and therefore the horizontal shear. The geometry for the upwelling jet, with the same coordinate system adopted for the two-layer, steady upwelling model on the Brazilian coast, is shown in Figure 2.

[26] The velocities presented in Figure 2 at $y = 0$ and at $y = -\Delta y$, as a function of x can be written as (with $v_0 < 0$ and $v_{-\Delta y} < 0$):

$$v(x, y = 0) = \begin{cases} v_0 \dfrac{x}{S}, & x \le S \\ 0, & x > S \end{cases}, \tag{16}$$

$$v(x, y = -\Delta y) = \begin{cases} v_{-\Delta y}\left(\dfrac{x - \Delta x}{S - \Delta x}\right), & x \le S \\ 0. & x > S \end{cases}. \tag{17}$$

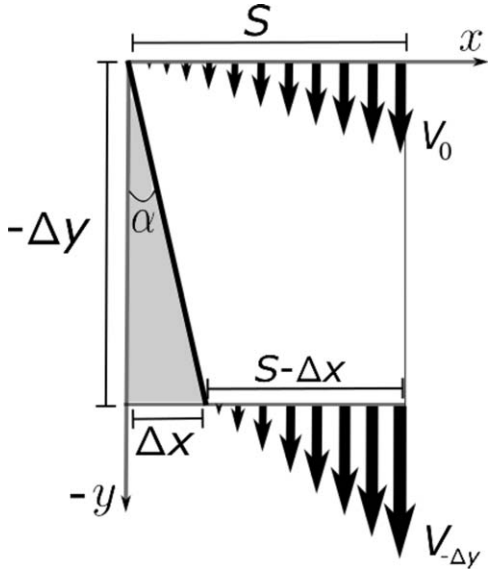

Figure 2. Geometry of the upwelling jet used for the calculation of vertical velocities induced by the changes of horizontal shear due to coastline irregularities.

[27] Note that $v(x=0,y=0)=0, v(x=S,y=0)=v_0$; and $v(x=\Delta x, y=-\Delta y)=0, v(x=S,y=-\Delta y)=v_{-\Delta y}$. Conservation of volume or the continuity equation, assuming the water is incompressible, can be written as:

$$\frac{1}{2}v_0 S = \frac{1}{2}v_{-\Delta y}(S-\Delta x), \tag{18}$$

so that $v_{-\Delta y}$ and v_0 are related by:

$$v_{-\Delta y} = v_0 \frac{S}{(S-\Delta x)}. \tag{19}$$

[28] The cross-shelf shear becomes:

$$\frac{\partial v(x,y=0)}{\partial x} = \frac{v_0}{S}, \tag{20}$$

$$\frac{\partial v(x,y=-\Delta y)}{\partial x} = \frac{v_{-\Delta y}}{S-\Delta x} = \frac{v_0 S}{(S-\Delta x)^2}. \tag{21}$$

[29] The along-shelf gradient in relative vorticity needed to compute the vertical velocities in (12) is:

$$\frac{\partial}{\partial y}\left(\frac{\partial v}{\partial x}\right) = \frac{\frac{\partial v(x,y=-\Delta y)}{\partial x} - \frac{\partial v(x,y=0)}{\partial x}}{\Delta y} = \frac{2Sv_0\Delta x - v_0\Delta x^2}{S\Delta y(S^2 - 2S\Delta x + \Delta x^2)}, \tag{22}$$

and using the geometric fact that $\Delta x = \Delta y \tan\alpha$

$$\frac{\partial}{\partial y}\left(\frac{\partial v}{\partial x}\right) = \frac{2Sv_0\tan\alpha - v_0\Delta y\tan^2\alpha}{S^3 - 2S^2\Delta y\tan\alpha + S\Delta y^2\tan^2\alpha}. \tag{23}$$

[30] In the limit $\Delta y \to 0$

$$\frac{\partial}{\partial y}\left(\frac{\partial v}{\partial x}\right) = \frac{2v_0\tan\alpha}{S^2}. \tag{24}$$

[31] The contribution from changes of horizontal shear due to topographic effects (w_{tshear}) in equation (12) becomes:

$$w_{tshear} = -\frac{Hv}{2f}\frac{\partial}{\partial y}\left(\frac{\partial v}{\partial x}\right) = -\frac{Hv_0 x}{2fS}\frac{2v_0\tan\alpha}{S^2} = -\frac{Hv_0^2 x}{fS^3}\tan\alpha. \tag{25}$$

[32] This term is slightly different than *Figueroa and Moffat* [1998], because we have retained full dependence in x, while the authors evaluated w_{tshear} at $x=S$.

[33] As discussed previously, changes in coastline curvature can also generate relative vorticity gradients, and therefore induce vertical velocities. This mechanism, not included by *Figueroa and Moffat* [1998], will also be included in our estimates, and can be calculated by using the definition of vorticity in natural coordinates from equation (13):

$$\begin{aligned} w_{tradius} &= -\frac{Hv}{2f}\frac{\partial\xi}{\partial y} = -\frac{Hv}{2f}\frac{\partial}{\partial y}\left(\frac{V}{R}\right) = -\frac{Hv_0 x}{2fS}\frac{\partial}{\partial y}\left(\frac{|v_0|x}{SR}\right) \\ &= -\frac{Hv_o|v_o|x^2}{2fS^2}\frac{\partial R^{-1}}{\partial y}, \end{aligned} \tag{26}$$

where R is the radius of the local coastline or R^{-1} the coastline curvature, and R can be either positive or negative, following the convention of positive R driving currents with positive vorticity (anticlockwise) and negative R driving currents with negative vorticity (clockwise).

[34] The total contribution to the upwelling vertical velocities (w_{total}) now has four terms (dropping subscripts in ρ for simplicity):

$$w_{total} = \underbrace{\overbrace{\frac{\tau_o^y}{\rho f \lambda_i}}^{w_{coastal}} + \overbrace{\frac{1}{2\rho f}\left(\frac{\partial\tau_o^y}{\partial x} - \frac{\partial\tau_o^x}{\partial y}\right)}^{w_{curl}}}_{\text{wind}} - \underbrace{\overbrace{\frac{Hv_o^2 x}{fS^3}tan\alpha}^{w_{tshear}} - \overbrace{\frac{Hv_o|v_o|x^2}{2fS^2}\frac{\partial R^{-1}}{\partial y}}^{w_{tradius}}}_{\text{topography}}. \tag{27}$$

[35] The choice of a proper coastal upwelling cross-shore length scale (λ_i) can be ambiguous and vary in space. One way to deal with this problem is by calculating an integrated version of equation (28) from the coast out to a distance L ($L > \lambda_i$ and $L > S$), where the total vertical transport (W_{total}) is given by:

$$\begin{aligned} W_{total} = &\underbrace{\overbrace{\frac{\tau_o^y}{\rho f}}^{W_{coastal}} + \overbrace{\int_0^L \frac{1}{2\rho f}\left(\frac{\partial\tau_o^y}{\partial x} - \frac{\partial\tau_o^x}{\partial y}\right)\mathrm{d}x}^{W_{curl}}}_{\text{wind}} \\ &\underbrace{-\overbrace{\frac{Hv_o^2}{2fS}tan\alpha}^{W_{tshear}} - \overbrace{\frac{Hv_o|v_o|S}{6f}\frac{\partial R^{-1}}{\partial y}}^{W_{tradius}}}_{\text{topography}}, \end{aligned} \tag{28}$$

where W's refer to the vertical transports in $\mathrm{m^3\ s^{-1}}$ per meter of coastline. The trade off for eliminating the length scale λ_i, is the appearance of a new length scale L for the integration of the Ekman pumping term (w_{curl}).

3. Data and Methods

[36] In order to understand the role of different upwelling mechanisms as well as the total upwelling transport (W_{total}) within two upwelling regions in Brazil, Cabo Frio, and Cabo de Santa Marta, each term of equation (23) was estimated, and comparisons with SST were made. The austral summer season (January, February, and March) was chosen for the analysis due to its quasi-steady nature, and therefore the applications of the two-layer, steady model are expected to be more realistic.

[37] For the wind contribution to the upwelling, climatological monthly wind stress and wind stress curl remote sensing data were obtained from *Risien and Chelton* [2001], based on an 8 year record (September 1999 to August 2007) from the SeaWinds Scatterometer on the QuikSCAT satellite. In all calculations, the summer mean and standard deviations were estimated from the climatological data of January, February, and March.

[38] Wind stress data from the SeaWinds Scatterometer are acquired daily, with a 25 km space resolution, covering over 90% of the global ocean surface, with accuracy better

than 2 m s^{-1} in speed and 20° in direction, which is essentially equivalent to the accuracy of in situ point measurements from buoys [*Freilich and Dunbar*, 1994]. The high-spatial resolution of the QuikSCAT scatterometer has revealed small-scale features of the global wind stress field that cannot be detected by any other means [*Chelton et al*., 1982]. A drawback of SeaWinds is the antenna sidelobe contamination, which leads to a data gap in the first 30 km close to the land. Further details about the SeaWinds Scatterometer can be found in *Freilich et al*. [1974] and *Chelton and Freilich* [2005].

[39] Ekman pumping driven vertical velocities were integrated from the coast up to the offshore distance L of 80 km. The length scale L was chosen to be the average shelf width for both study regions, due its ecological relevance for nutrient enrichment and primary productivity on the continental shelves. The coastal band where there is a data gap from the SeaWinds Scatterometer, was filled up by extrapolating the wind stress curl data through nearest-neighbor method.

[40] The coastline data, used in the calculations of Ekman transport and upwelling due to changes in horizontal shear as well as due to changes in flow curvature, were obtained from World Data Bank II (designed for 1:2,000,000) from National Geophysical Data Center—NOAA (http://www.ngdc.noaa.gov/mgg/coast/). The data were interpolated to 10 km resolution and smoothed by a running average of 30 km applied twice.

[41] In order to determine the orientation of the coastline for the Ekman transport calculation, straight lines were fitted through least squares, spanning 50 km of coastline centered at the wind stress grid points. Changes in coastline orientation for the calculation of upwelling driven by changes in horizontal shear were estimated by first-order differencing the coastline data. For the upwelling driven by changes in flow curvature, coastline radii (Figure 3) were

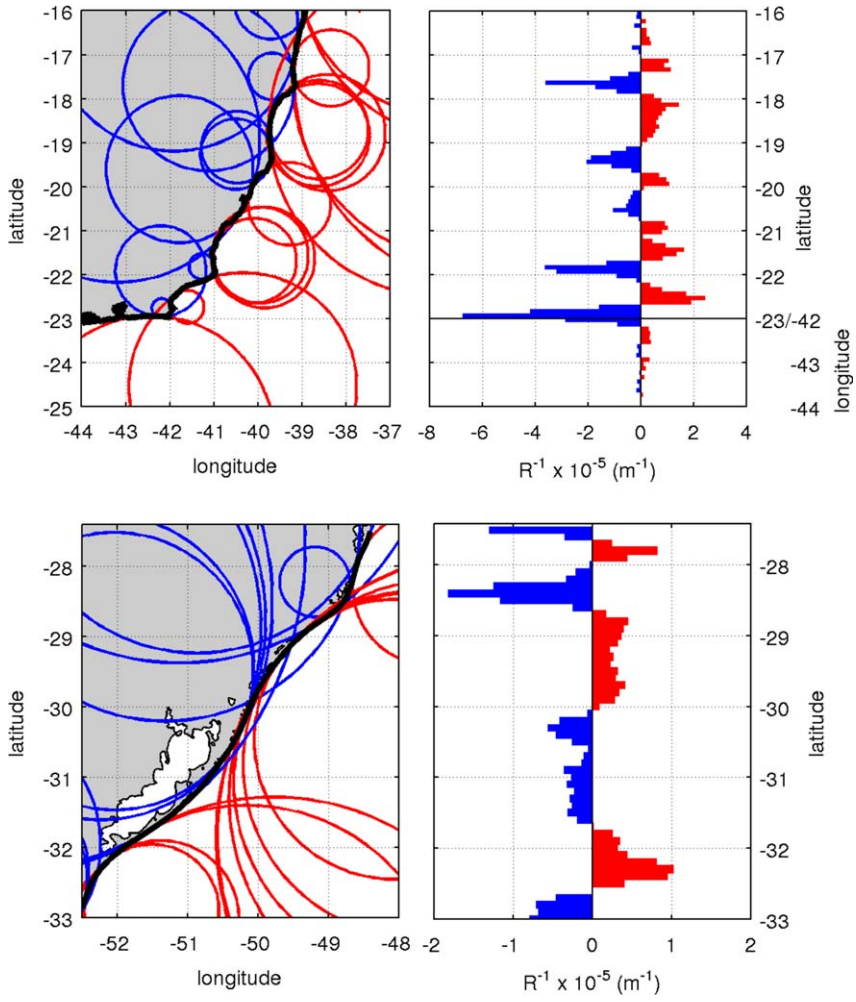

Figure 3. (left) Circles fitted to the coastline of the regions of (top) Cabo Frio and (bottom) Cabo de Santa Marta (only a few circles with radius smaller than 500 km were selected for better visualization); (right) coastline curvature ($1/R$). Blue refers to curvature driving currents with negative vorticity (cyclonic) and red refers to curvature driving currents with positive vorticity (anticyclonic), for a southward upwelling jet. The y axis coordinate system in the top right plot (Cabo Frio region) changes from a function of latitude from 16°S to 23°S to a function of longitude from 42°W to 44°W and the two regions are separated by a black straight line.

estimated by fitting circles using least squares centered at each coastal grid point and using the previous and next point, a total of three coastline points (fits with five and seven points were also tested and did not change the results significantly).

[42] Finally, the constant parameters used in our calculations were: $\rho = 1025\,\mathrm{kg\ m^{-3}}$; $v_o = 0.15 \pm 0.05\,\mathrm{ms^{-1}}$; $H = 70\,\mathrm{m}$; $S = 35\,\mathrm{km}$. All results were smoothed out by a 30 km span running mean. These are reasonable values according to coastal upwelling physics, and agree well with parameters from previous works done in these regions.

[43] *Rodrigues and Lorenzzetti* [2001] obtained from model results typical longshore velocities of 0.14 m s^{-1} in the upper layer of the regions between Cabo Frio and Vitória (V). The mean depth of the region is approximately 70 m, being the value the authors adopted for the flat-bottom simulations. The coastal jet in their model showed cross-shelf length scales varying from 30 to 40 km, hence our choice of $S = 35$ km.

[44] An analytical model for the southern Brazilian shelf (between 29°S and 35°S) from *Pereira* [2000] show surface currents on the order of 0.1 m s^{-1} during summer. Numerical simulations for the region of the South Brazil Bight by *Palma and Matano* [1989], using a full primitive equations model under realistic forcing conditions, presented velocities ranging from 0.05 to 0.1 m s^{-1} near the bottom, and from 0.2 to 0.4 m s^{-1} on the surface for the shallower regions between 27°S and 29°S near Cabo de Santa Marta and Ilha de Santa Catarina, during summer. *Campos et al*. [2013] presented results from numerical simulations at Cabo de Santa Marta region with velocities ranging between 0.1 and 0.2 m s^{-1} near the coast.

[45] Therefore, values chosen for Cabo Frio are also valid for Cabo de Santa Marta. We assumed same jet width (S) and mean depth as used for Cabo Frio, since the shelf at Cabo de Santa Marta presents similar geometry as the average region between Cabo Frio and Cabo de São Tomé.

[46] Due to the lack of observational data and uncertainties of longshore currents, we attributed a variation of ± 0.05 m s^{-1} around the central value chosen (0.15 m s^{-1}), which corresponds to nearly 33% of variability. Variations of longshore velocities will cause variations in topographically driven upwelling transport proportional to the square of v_o as can be seen in equation (23).

[47] In the climatological SST from the Advanced Very High Resolution Radiometer (NOAA AVHRR v2), (Figure 1) it is possible to observe large-scale seasonal variability along the Brazilian coast, however mesoscale SST features associated with topographic and coastline variations are masked due to smoothing and averaging over the highly dynamic coastal environment.

[48] In order to capture mesoscale SST variability along the coast, higher resolution (5.5 km), daily, gap-free SST images from the "Operational Sea Surface Temperature and Sea Ice Analysis" (OSTIA) from 1998 to 2007 as well as the OSTIA reanalysis from 2009 to present [*Stark et al*., 1992] were used.

[49] Periods when upwelling was persistent for at least 7 days were chosen and then SST images were averaged over that time. Direct comparisons were made between the vertical transports and the SST data closest to the coast, where coldest SSTs are often observed. Both low-passed and high-passed (boxcar filters with width of 181.5 km for CF and 225.5 km for CSM) SST data along the coast were compared to different upwelling mechanisms, in order to understand their along-shelf spatial scales.

[50] To aid in the characterization of upwelling events and understand the general circulation, absolute geostrophic velocity fields computed from satellite-derived absolute sea surface height were analyzed. The altimeter products used in this paper were produced by Ssalto/Duacs and distributed by Aviso, with support from Cnes (http://www.aviso.oceanobs.com/duacs/).

[51] To verify that the individual weeks of SST selected for comparison with vertical transport estimates were typical of coastal upwelling off Brazil, as well as to understand the variance explained due to upwelling events over the regions of Cabo Frio and Cabo de Santa Marta, the continuous time series of SST data from 1998 to 2007 were decomposed into Empirical Orthogonal Functions (EOFs). To perform the EOF analysis, first each SST image had the latitudinal trend in SST removed by normalizing the temperature at each latitude by subtracting the maximum temperature located along the shelf break (between 200 m and 2000 m isobaths), where the Brazil current is roughly located. After removal of the latitudinal trend, the seasonal cycle was also removed using harmonic analysis (five parameters: mean, annual, and semiannual), and finally, the summer months (January, February, and March) were used in the EOF decomposition.

4. Results

4.1. Cabo Frio Region

[52] The average sea surface temperature (°C) between the 25th and 31th of March 2012, obtained from the "Operational Sea Surface Temperature and Sea Ice Analysis" (OSTIA), overlayed by absolute geostrophic velocity field computed from satellite-derived absolute sea surface height for 28th of March 2012, are shown in Figure 4 (top, left). The EOF first mode explains 30.9% of the total variance (Figure 4, bottom, left), and closely resembles upwelling event shown in the SST image from OSTIA. The geostrophic currents flow southward along the coast, with velocities varying roughly from 0.2 to 0.5 m s^{-1}. Further comparisons are made between the SST along the coast and the total vertical transport (below).

[53] The results for vertical transports within the Cabo Frio (CF) region are shown in Figure 5. A detailed map of the region is presented in Figure 5a, covering from south of Cabo Frio around 23°S up to 16°S. The shelf geometry is quite complex, with highly variable shelf width: 50 km at Cabo Frio, 80 km between Cabo Frio and Cabo de São Tomé (CST), 40 km at Vitória (V), 100–240 km between Rio Doce (RD) and Caravelas (CA), and 45 km north of Caravelas.

[54] Topographically driven upwelling transports including those due to changes in coastline curvature, $W_{tradius}$ in red, as well as those due to changes in horizontal shear, W_{tshear} in green, are presented in Figure 5b. The solid lines represent the values estimated using $v = 0.15$ m s^{-1} and the shaded areas represent uncertainties obtained through using $v = 0.15 \pm 0.05$ m s^{-1}, to give upper and lower bounds. Both mechanisms, $W_{tradius}$ and W_{tshear}, are highly variable

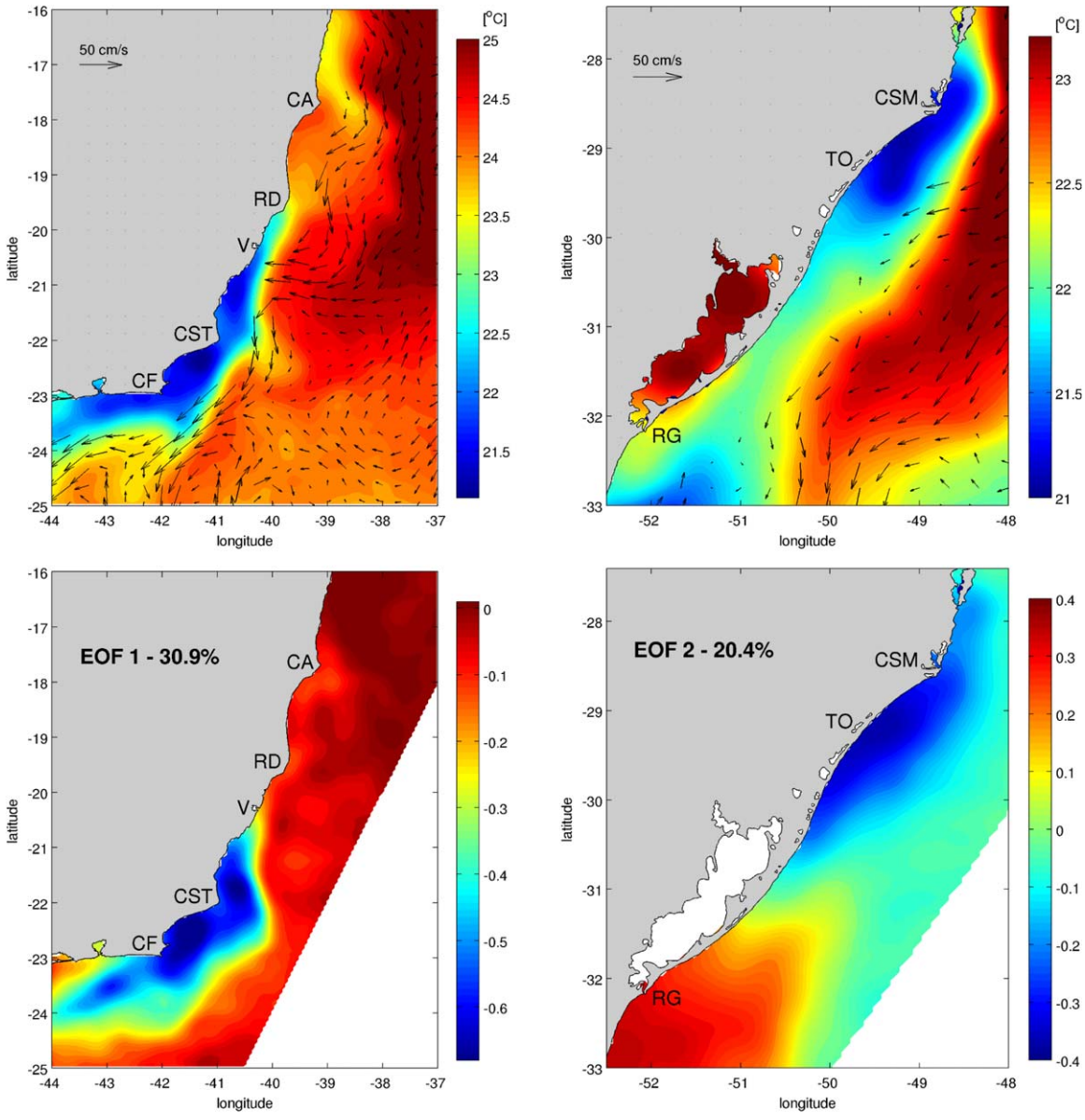

Figure 4. (top) Sea surface temperature (SST) from the "Operational Sea Surface Temperature and Sea Ice Analysis" (OSTIA) overlayed by absolute geostrophic velocity field computed from satellite-derived absolute sea surface height (first 50 km near the coast were masked due to land contamination) for the regions of: (left) Cabo Frio, with SST averaged between the 25th and 31th of March 2012, and absolute geostrophic currents for 28th of March 2012 (CF: Cabo Frio; CST: Cabo de São Tomé; V: Vitória; RD: Rio Doce; CA: Caravelas); (right) Cabo de Santa Marta, with SST averaged between the 13th and 19th of March 2012, and absolute geostrophic currents for 14th of March 2012 (CSM: Cabo de Santa Marta; TO: Torres; RG: Rio Grande). (bottom) Empirical Orthogonal Functions calculated from daily OSTIA SST images for the summer months (January, February, and March) from 1998 through 2007 (10 years), after removed latitudinal dependence and seasonal cycle. Percentage of variance and mode number are shown in each plot.

along the coast, changing sign from positive to negative several times, and tending to zero west of Cabo Frio. Upwelling due to flow curvature ($W_{tradius}$) has a mean close to zero (-0.5×10^{-2} m^2 s^{-1}), and four main, nearly symmetric transitions from a negative to a positive peak: at Caravelas, Rio Doce, Cabo de São Tomé, and Cabo Frio. The amplitudes of the transition peaks at Caravelas, Rio Doce and Cabo de São Tomé range approximately from 0.1 to 0.2 ($\pm 0.08-0.13$) m^2 s^{-1} whereas at Cabo Frio the peaks are almost twice as large, 0.4 (± 0.28) m^2 s^{-1}.

[55] Upwelling due to along-shelf changes in shear (W_{tshear}) has a mean value close to zero (0.7×10^{-2} m^2 s^{-1}) and shows five positive and five negative peaks, being non-symmetric around zero, with the positive amplitudes about two times larger than the amplitudes of the negative peaks. The negative peaks are located slightly north of Caravelas,

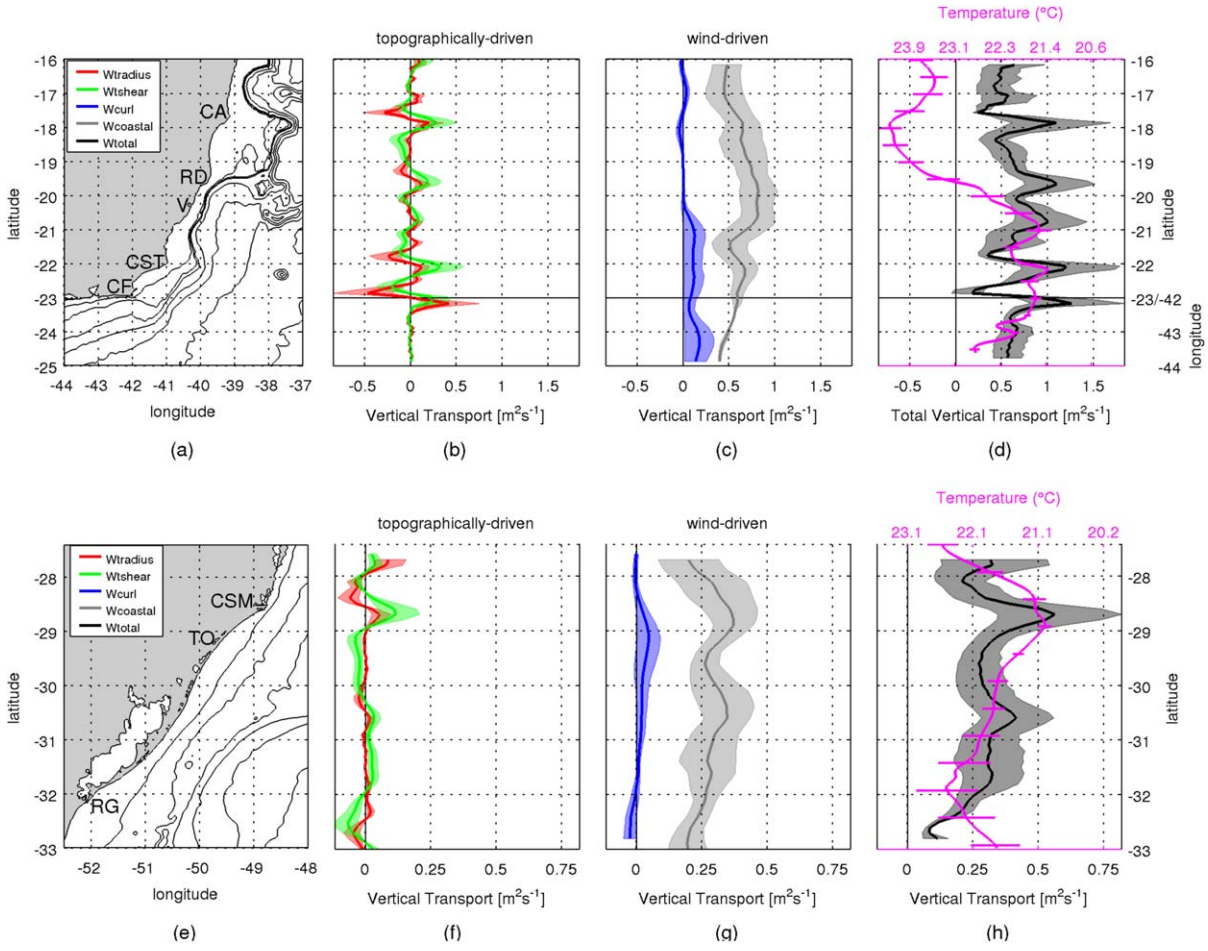

Figure 5. Vertical transports calculated in the vicinity of (top) Cabo Frio (CF) region and (bottom) Cabo de Santa Marta (CSM) region, Brazil. Transports are presented as $m^3\ s^{-1}$ per m of coastline. (a) Cabo Frio and (e) Cabo de Santa Marta region maps, showing isobaths of 50, 100, 200, 1000, 2000, 3000, and 4000 m. Legends on the left refer to subsequent plots. (CF: Cabo Frio; CST: Cabo de São Tomé; V: Vitória; RD: Rio Doce; CA: Caravelas; CSM: Cabo de Santa Marta; TO: Torres; RG: Rio Grande); (b and f) Topographically driven vertical transports along the coast. Green refers to W_{tshear} and red to $W_{tradius}$. Upper and lower limits of shaded areas correspond to the calculations using $v = 0.15 \pm 0.05$ m s^{-1}. (c and g) Wind-driven vertical transports along the coast. Blue refers to W_{curl} and light gray to $W_{coastal}$. Upper and lower limits of shaded areas correspond to one standard deviation from the summer (January, February, and March) mean. (d and h) Total upwelling transports and sea surface temperatures along the coast. Dark gray refers to W_{total} and magenta refers to temperature in °C, averaged between the 25th and 31th of March 2012 in Figure 5d and between the 13th and 19th of March 2012 in Figure 5h obtained from the "Operational Sea Surface Temperature and Sea Ice Analysis" (Figure 4, top). Note that temperature scales are reversed for better visualization. The y axis coordinate system for Figures 5b–5d changes from a function of latitude from 16°S to 23°S to a function of longitude from 42°W to 44°W and the two regions are separated by a black straight line.

Rio Doce, Vitória, Cabo de São Tomé, and Cabo Frio, with values ranging from −0.09 to −0.13 (±0.06−0.09) $m^2\ s^{-1}$ between Caravelas and Cabo de São Tomé, and the largest peak between Cabo de São Tomé and Cabo Frio, with −0.2 (±0.15) $m^2\ s^{-1}$. Positive peaks are located slightly south of Caravelas, Rio Doce, Vitória, Cabo de São Tomé, and Cabo Frio, where the smallest peak south of Vitória has amplitude of 0.08 (±0.05) $m^2\ s^{-1}$, followed by the peak south of Rio Doce with 0.18 (±0.12) $m^2\ s^{-1}$, then Cabo Frio with 0.24 (±0.15) $m^2\ s^{-1}$, Caravelas with 0.28 (±0.18) $m^2\ s^{-1}$, and finally Cabo de São Tomé with largest peak of 0.32 (±0.21) $m^2\ s^{-1}$.

[56] The wind-driven vertical transports show both coastal upwelling, $W_{coastal}$ in gray, and Ekman-pumping driven transport, W_{curl} in blue (Figure 5c). The darker line represents the summer mean along-shelf vertical transports obtained from January, February, and March monthly climatological wind stress values and shaded areas denote the mean ±1 standard deviation. Coastal upwelling ($W_{coastal}$) is relatively uniform over the region and upwelling favorable, with a mean value of 0.6 (±0.2) $m^2\ s^{-1}$. Largest transports are found in the region between Vitória and Rio Doce, 0.75 (±0.2) $m^2\ s^{-1}$, and then decay toward both the north and south, with lowest values found at the southern

limit of the domain, 0.4 ($\pm$0.03) m^2 s^{-1}. Ekman pumping upwelling transports (W_{curl}) are much smaller than coastal upwelling ($W_{coastal}$), with an average value of 0.05 ($\pm$0.06) m^2 s^{-1}. Upwelling due to wind stress curl is nearly zero north of Vitória, and nearly 0.12 ($\pm$0.1) m^2 s^{-1} south of Vitória.

[57] The total vertical transports, wind-driven plus topographically driven, W_{total}, are shown in Figure 5d with the mean (black solid line) and the variation (gray shaded area) obtained from the sum of all lower and upper bounds of the individual vertical transport terms. The average sea surface temperature (°C) along the coast between the 25th and 31th of March 2012, from Figure 4 (top, left), is shown in dash-dotted line, with upper and lower bounds being the mean $\pm$1 standard deviation. The total vertical transport (W_{total}) has a mean value of 0.68 ($\pm$0.22) m^2 s^{-1}, is highly variable and upwelling favorable (positive) in the entire region.

[58] Two major upwelling peaks are found south of Cabo de São Tomé with 1.19 ($\pm$0.53) m^2 s^{-1}, and south of Cabo Frio with 1.25 ($\pm$0.53) m^2 s^{-1}, and other three peaks of slightly smaller magnitudes are found (in increasing size): south of Vitória, 1 ($\pm$0.47) m^2 s^{-1}, Caravelas 1.09 ($\pm$0.53) m^2 s^{-1}, and Rio Doce 1.1 ($\pm$0.38) m^2 s^{-1}.

[59] The temperature along the coast shows a maximum of nearly 24.4°C near Caravelas (18°S), where the shelf is widest, then slowly decreases from Caravelas to Rio Doce as a response of an upwelling peak just south of Caravelas. Further decrease in SST, at a higher rate, occur from Rio Doce, where the shelf narrows down, to 21°S, responding to two consecutive upwelling peaks at Rio Doce and Vitória. Between 21°S and just to the west of Cabo Frio, there are three SST oscillations of up to 0.5°C around 21.5–22°C, with lowest temperature peaks occurring slightly southward of the upwelling velocity peaks. SST then warms up westwards of 42.5°S.

[60] In order to further understand the relationship between SST and vertical transport, comparisons between vertical transports driven by topography-flow interaction and high-passed SST along the coast, as well as between vertical wind-driven transports and low-passed SST along the coast are presented in Figure 6. A maximum significant correlation of -0.31 (95% confidence level of -0.25) is found between high-passed SST and vertical transports driven by topography-flow interaction at the lag of 16.6 km, where the cold water is found downstream of the capes.

[61] To understand the role played by topography versus wind in driving vertical transports, the ratio between topographically driven and wind-driven upwelling transports is presented in Figure 7. Values smaller than one represent wind-driven upwelling, values larger than one represent topographically driven upwelling, and values equal to one show that the two mechanisms are equally important.

[62] In the entire domain, the ratio is smaller than one, so wind is the major forcing mechanism. North of Cabo de São Tomé, the ratio is approximately 0.5, where the topographic effects are half of the wind contribution. Places where the flow-topography interactions represent over half of the wind contribution are: south of Cabo de São Tomé with ratio of 0.57, north of Caravelas with 0.58, north of Cabo Frio with 0.73, south of Caravelas wit 0.78, and north of Cabo Frio 0.94, where topographically driven upwelling becomes nearly as important as wind-driven upwelling.

4.2. Cabo de Santa Marta Region

[63] The average sea surface temperature (°C) between the 13th and 19th of March 2012, obtained from OSTIA, overlayed by absolute geostrophic velocity field computed from satellite-derived absolute sea surface height for 14th of March 2012, are shown in Figure 4 (top, right). The EOF first mode (not shown) explains 34.7% of the total variance, and resembles intrusion of cold waters from the south [*Pereira*, 2000; *Campos et al*., 1996; *Lima et al*., 1979; *Campos et al*., 1999; *Piola et al*., 2005; *Lentini et al*., 1996; *Soares and Möller*, 2004; *Zavialov et al*., 2002; *Souza and Robinson*, 2007; *Piola et al*., 2008, 2008] while the second mode (Figure 4, bottom, right) explains 20.4% of the total variance and closely resembles upwelling events south of Cabo de Santa Marta, such as the one shown in the SST image from OSTIA. The geostrophic currents flow southwestward along the coast in the vicinities of Cabo de Santa Marta, with velocities varying roughly from 0.2 to 0.4 m s^{-1}, while south of Torres, they become weaker with no clear preferable direction. Midway between Torres and Rio Grande they increase their velocities again, and in the vicinities of Rio Grande they become weaker and reverse direction in the southern end of the domain. Further comparisons are made between the SST along the coast and the total vertical transport (below).

[64] The results for vertical transports for Cabo de Santa Marta (CSM) region are shown in Figure 5. A detailed map of the region is presented in Figure 5e, covering from south of Rio Grande (RG), 33°S, up to the north of Cabo de Santa Marta, reaching Ilha de Santa Catarina, 27.4°S. The shelf geometry is quite smooth, oriented in the NE-SW direction, with isobaths tending to follow the coastline, and having the most abrupt disturbance at Cabo de Santa Marta, where the coastline changes its mean orientation. Shelf width is around 70 km at Cabo de Santa Marta, then it widens up southward with an average of 110 km, and then reaches its maximum width of 170 km at the southward end of the domain, just south of Rio Grande.

[65] Topographically driven upwelling transports including those due to changes in coastline curvature, $W_{tradius}$ in red, as well as those due to changes in horizontal shear, W_{tshear} in green, are presented in Figure 5f. The solid lines represent the values estimated using $v = 0.15$ m s^{-1} and the shaded areas represent uncertainties obtained through using $v = 0.15 \pm 0.05$ m s^{-1}, to give upper and lower bounds. Both mechanisms, $W_{tradius}$ and W_{tshear}, start with positive values of similar magnitudes in the northern border of the domain, of around 0.05 ($\pm$0.02) m^2 s^{-1}, and becoming negative southward of 28°S, reaching -0.05 ($\pm$0.02) m^2 s^{-1}, with $W_{tradius}$ having a broader peak. There is a positive narrow peak in $W_{tradius}$ south of Cabo de Santa Marta, with a magnitude of 0.05 ($\pm$0.04) m^2 s^{-1}, and then $W_{tradius}$ becomes nearly zero southward of 29°S, until the southern border, when there is a negative peak of -0.05 ($\pm$0.03) m^2 s^{-1}.

[66] W_{tshear} reaches its highest value slightly south of Cabo de Santa Marta of 0.12 ($\pm$0.08) m^2 s^{-1}, then it becomes negative at Torres (TO), -0.03 ($\pm$0.02) m^2 s^{-1}, and turns to positive halfway until Rio Grande, 0.02 ($\pm$0.02) m^2 s^{-1}. South of Rio Grande, it reaches its negative highest peak of -0.06 ($\pm$0.04) m^2 s^{-1}. Upwelling due to flow curvature ($W_{tradius}$) has a mean close to zero (0.8 $\times$

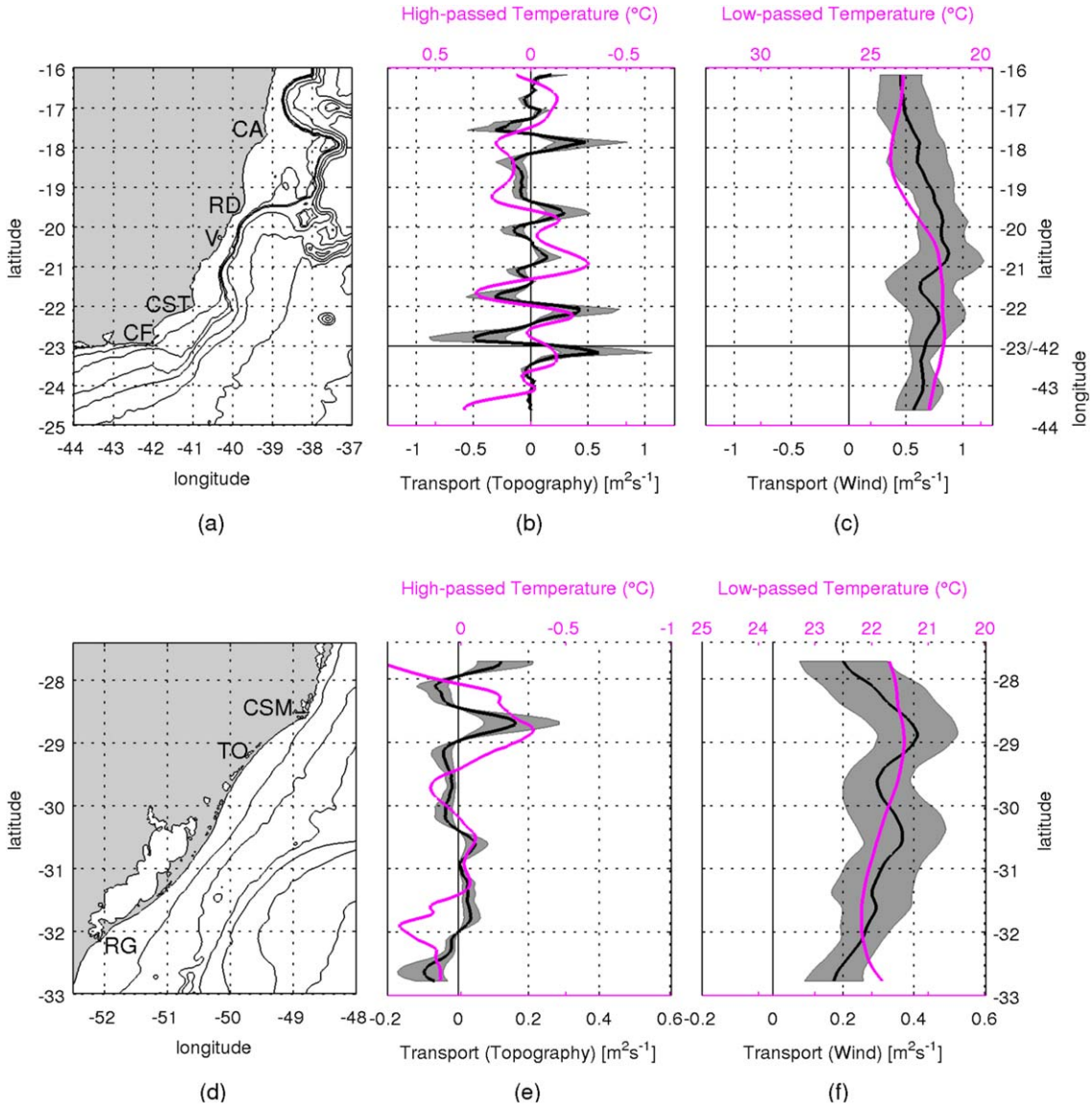

Figure 6. Comparisons (b and e) between vertical transports driven by topography-flow interaction and high-passed SST along the coast, and (c and f) between vertical wind-driven transports and low-passed SST along the coast, for (top) Cabo Frio (CF) region and (bottom) Cabo de Santa Marta (CSM) region, Brazil. Transports are presented as $m^3\ s^{-1}$ per m of coastline (dark gray), and temperature (magenta) in °C, averaged between the 25th and 31th of March 2012 in Figures 6b and 6c and between the 13th and 19th of March 2012 in Figures 6e and 6f obtained from the "Operational Sea Surface Temperature and Sea Ice Analysis" (Figure 4, top). The *y* axis coordinate system for Figures 6b and 6c changes from a function of latitude from 16°S to 23°S to a function of longitude from 42°W to 44°W and the two regions are separated by a black straight line. Note that temperature scales are reversed for better visualization.

10^{-3} $m^2\ s^{-1}$), while upwelling due to changes in horizontal shear has a mean value of 0.6×10^{-2} $m^2\ s^{-1}$, one order of magnitude higher.

[67] The wind-driven vertical transports show both coastal upwelling, $W_{coastal}$ in gray, and Ekman-pumping transports, W_{curl} in blue (Figure 5g). The darker line represents the summer mean along-shelf vertical transports obtained from January, February, and March monthly climatological wind stress values and shaded areas denote the mean ± 1 standard deviation. Coastal upwelling ($W_{coastal}$) is relatively uniform over the region and upwelling favorable, with a mean value of 0.28 (±0.08) $m^2\ s^{-1}$. Largest upwelling transports are found just south of Cabo de Santa Marta, 0.37 (±0.07) $m^2\ s^{-1}$, and approximately at 30.5°S, 0.34 (±0.09) $m^2\ s^{-1}$, then decreasing toward the northern border of the domain, 0.2 (±0.11) $m^2\ s^{-1}$, and southern border of the domain, 0.22 (±0.09) $m^2\ s^{-1}$.

[68] Ekman pumping upwelling transports (W_{curl}) are much smaller than transports due to coastal upwelling ($W_{coastal}$), with an average value of 0.01 (±0.02) $m^2\ s^{-1}$.

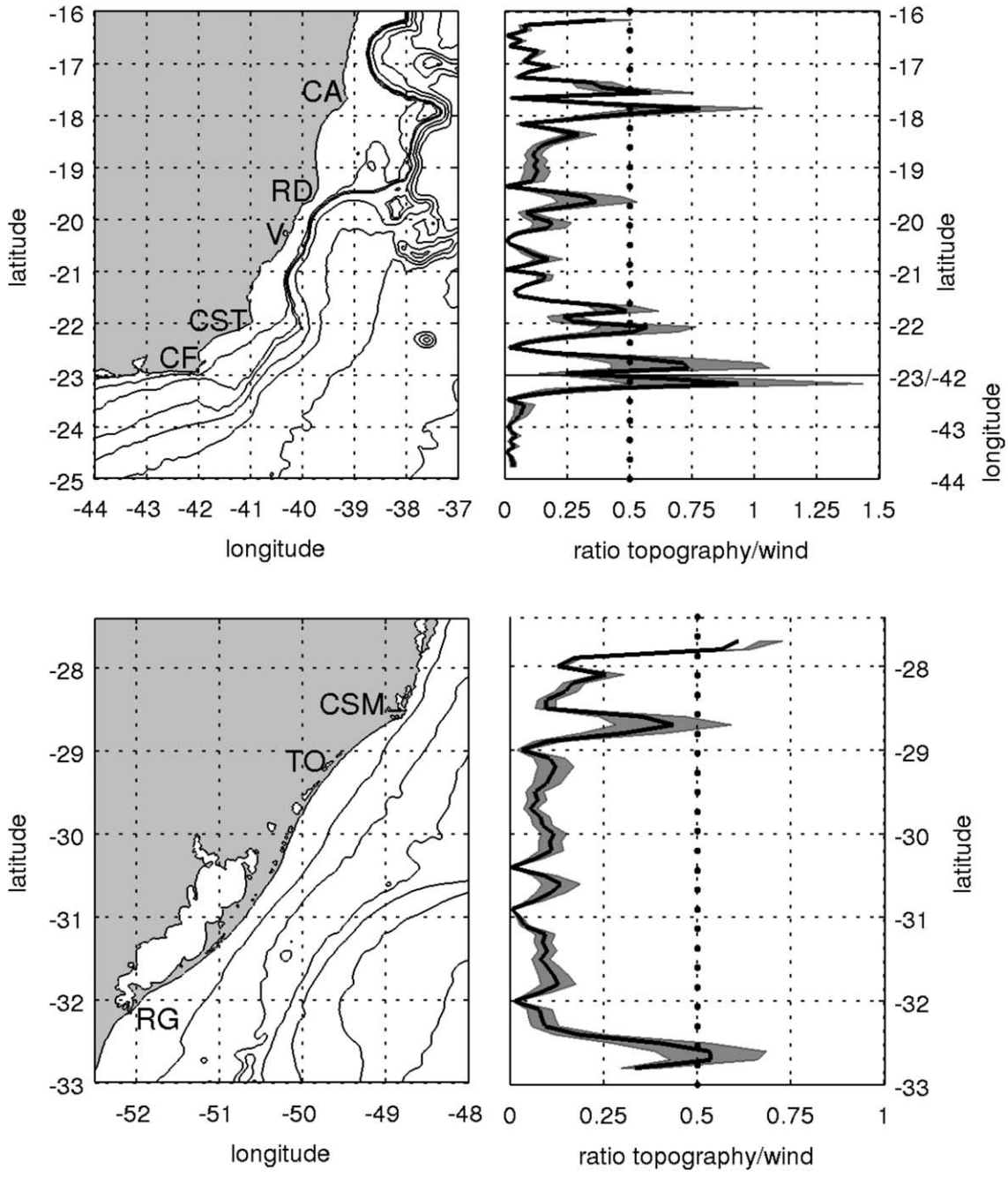

Figure 7. For the regions of (top) Cabo Frio and (bottom) Cabo de Santa Marta: maps (left), showing isobaths of 50, 100, 200, 1000, 2000, 3000, and 4000 m; ratio between topographically driven and wind-driven vertical transports (right). Dotted line points where contributions of topographically driven upwelling reach 50% of the wind-driven contribution. The *y* axis coordinate system for top right plot changes from a function of latitude from 16°S to 23°S to a function of longitude from 42°W to 44°W and the two regions are separated by a black straight line. (CF: Cabo Frio; CST: Cabo de São Tomé; V: Vitória; RD: Rio Doce; CA: Caravelas; CSM: Cabo de Santa Marta; TO: Torres; RG: Rio Grande.)

Positive values are found between Cabo de Santa Marta and 50 km north of Rio Grande, with maximum peak reaching 0.04 ($\pm$0.04) m^2 s^{-1}, while beyond this region values are slightly negative, downwelling favorable, with maximum value in the southern end of the domain, of -0.02 ($\pm$0.02) m^2 s^{-1}.

[69] The total vertical transports, wind-driven plus topographically driven, W_{total}, are shown in Figure 5h with the mean (black solid line) and the variation (gray shaded area) obtained from the sum of all lower and upper bounds of the individual vertical transport terms. The average sea surface temperature (°C) along the coast between the 13th and 19th

of March 2012, from Figure 4 (top, right), is shown in dash-dotted line, with upper and lower bounds being the mean ± 1 standard deviation. The total vertical transports (W_{total}) has a mean value of 0.3 (±0.1) $m^2\ s^{-1}$, and is upwelling favorable (positive) in the entire region.

[70] In the northern part of the domain, vertical transports are 0.3 (±0.2) $m^2\ s^{-1}$, quickly dropping to 0.2 (±0.1) $m^2\ s^{-1}$ just north of Cabo de Santa Marta, then reaching the largest peak south of Cabo de Santa Marta of 0.56 (±0.23) $m^2\ s^{-1}$. Southward of the maximum upwelling peak, transports are about 0.28 (±0.07) $m^2\ s^{-1}$, then halfway between Torres and Rio Grande they increase up to about 0.4 (±0.12) $m^2\ s^{-1}$ until they reach Rio Grande, decreasing after that.

[71] The temperature along the coast shows a maximum in the northern border, 22.6°C, and decreases rapidly until reaches its minimum value of 21.1°C, just south of the maximum upward transport peak south of Cabo de Santa Marta. The temperature then increases until it reaches 22.5°C just north of Rio Grande, and then decays southward to 21.7–21.8°C in the most southern limit of the domain.

[72] Comparisons between vertical transports driven by topography-flow interaction and high-passed SST along the coast, as well as between vertical wind-driven transports and low-passed SST along the coast are presented in Figure 6 (bottom). A maximum correlation of −0.44 (not statistically significant within 95% confidence level: −0.53) is found between high-passed SST and vertical transports driven by topography-flow interaction at the lag of 33.3 km, where cold water is found downstream of the capes.

[73] The ratio between topographically and wind-driven upwelling shows that wind is the main forcing mechanism for upwelling in most of the domain (Figure 8). The role of topography however, can be important in three different discrete places: in the northern part of the domain, where ratio is about 0.6, southern parts of the domain, with ratio 0.53, and just south of Cabo de Santa Marta, with ratio of 0.43.

5. Discussion

[74] The wind plays a fundamental role in both major upwelling systems of Brazil, Cabo Frio (CF) and Cabo de Santa Marta (CSM). During summer, the mean wind stress is directed toward the southwest (Figure 1), creating offshore Ekman transport (upwelling favorable) along the entire coast within these regions, and as a response, coastal upwelling is observed everywhere (Figure 5). This allows a southward, alongshore, upwelling jet to set up, and further create vertical velocities through the relative vorticity field gradients created by flow-topography interaction. As a direct effect of the stronger wind stress over the Cabo Frio region, its coastal upwelling is over two times larger than the coastal upwelling observed at Cabo de Santa Marta.

[75] An Empirical Orthogonal Function (EOF) analysis was used to describe variability in the SST upwelling signature along the coast. Near Cabo Frio (CF) upwelling was described by the first mode and represents 31% of the variability, however in Cabo de Santa Marta (CSM), the upwelling was better captured by the second mode, with 20% of variability. In the CSM region, northward advection of cold waters from the south seems to be the major factor responsible for controlling SST variability. In both regions, cold waters in the vicinity of coastal features are associated with a southward geostrophic flow, a typical characteristic of a coastal upwelling phenomenon off the Brazilian coast. It has been demonstrated at Cabo Frio that upwelling can have a significant impact on the coastal marine ecosystem, bringing nutrients to the surface water and enhancing fisheries productions [*Matsuura*, 1998, 1982].

[76] Ekman pumping has a nearly negligible impact on the vertical transports observed north of Vitória (CF region) and over most of the continental shelf within Cabo de Santa Marta region (except for a relatively small domain around 100 km centered at Torres), being in general one to two orders of magnitude smaller than coastal upwelling or topographic effects. However, significant contributions occur from south of Vitória to the southern end of the Cabo Frio region, where wind stress curl-driven upwelling reaches 15%, 30–50%, and 30–100% of the coastal upwelling, due to changes in horizontal shear, and due to changes in coastline curvature, respectively. A significant contribution of wind stress curl-driven upwelling is also found in the Cabo de Santa Marta region, at Torres, where it reaches 15%, 30%, and 90% of the coastal upwelling, upwelling due to changes in horizontal shear, and due to changes in coastline curvature, respectively.

[77] Despite its smaller contribution to the vertical transport over the continental shelves, negative wind stress curl (upwelling-favorable) is observed over a much larger extent offshore of the continental shelf. The net effect of this larger scale Ekman pumping, including the offshore region of negative wind stress curl (from the coast to approximately 200 km offshore) was shown by *Castelão and Barth* [2006b] to play a significant role in the vertical volume transport, along a ∼800 km wide coastal strip in the Cabo Frio region (between Vitória and São Sebastião). According to the authors, the vertical transport from wind stress curl driven upwelling has the same order of magnitude as vertical transport due to coastal upwelling.

[78] In this paper, we restricted our analysis of Ekman pumping to the continental shelf because we are interested in enhancement of primary productivity for the continental shelf marine ecosystem. Also, note that the Ekman pumping velocities (w_{curl}) calculated in this paper are different from the traditional $1\frac{1}{2}$-layer model $w = \hat{k} \cdot \nabla \times \frac{\vec{\tau_o}}{\rho f}$ [e.g., *Castelão and Barth*, 2006b; *Campos et al*., 2013] by a factor of two through the use of a two-layer model.

[79] It should be kept in mind that the wind stress and wind stress curl data in this paper miss the first 30 km near the coast due to a gap in the QuikSCAT satellite coverage, and that this gap was filled up by extrapolating the closest data point from offshore. This region is important for upwelling dynamics because both the Ekman pumping and Ekman transport (coastal upwelling) mechanisms are sensitive to the coastal wind profiles. According to *Capet et al*. [2004], high nearshore dropoff in the alongshore winds favors Ekman pumping, while stronger nearshore winds favor intense and localized coastal upwelling. This indicates that future investigation should be addressed to understand the spatial dependence of the nearshore wind field along the Brazilian coast, in order to fully understand the role played by these two mechanisms.

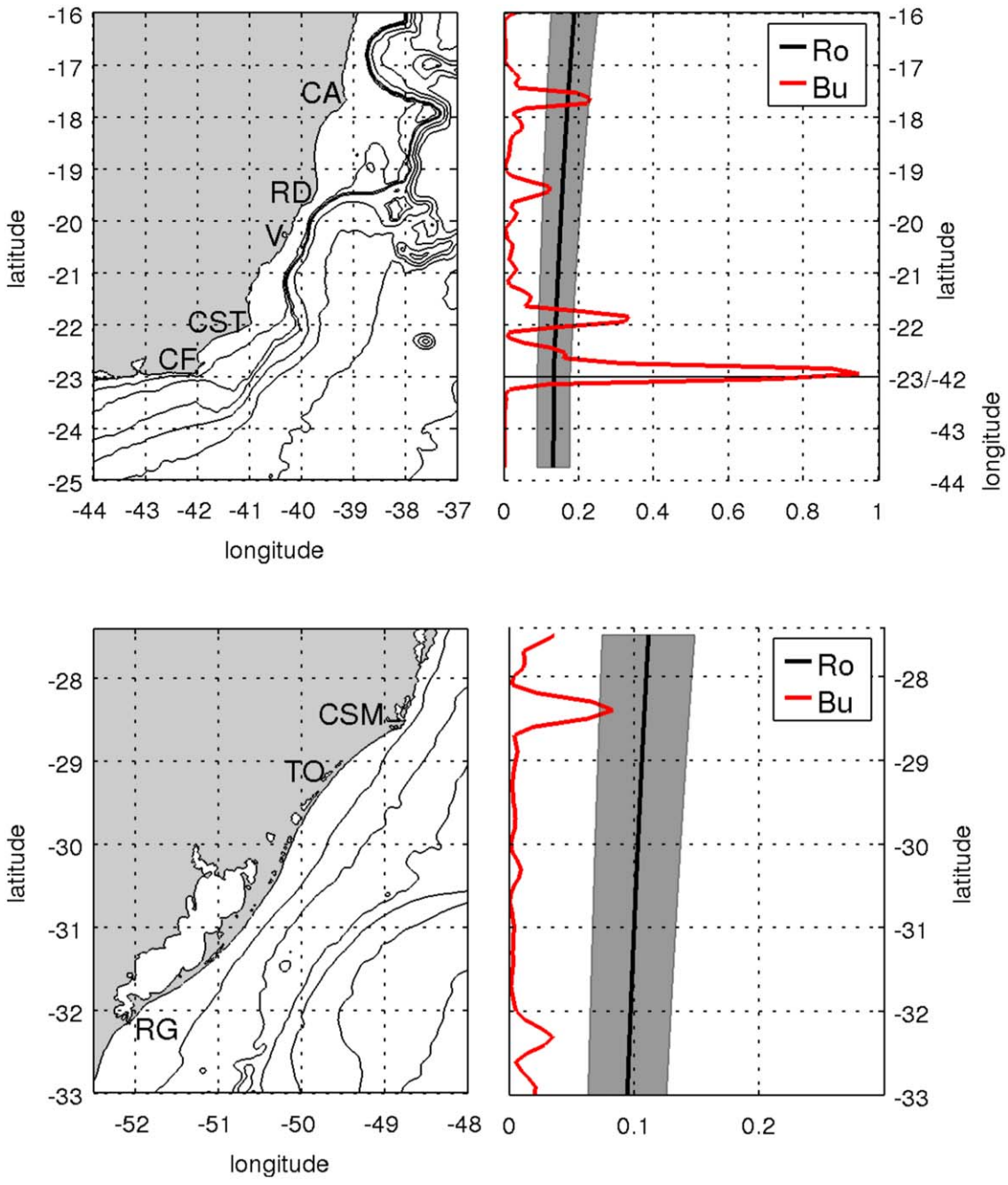

Figure 8. For the regions of (top) Cabo Frio and (bottom) Cabo de Santa Marta: maps (left), showing isobaths of 50, 100, 200, 1000, 2000, 3000 and 4000 m; jet separation criteria (right): Burger number (*Bu*) in red, and Rossby number (*Ro*) in black with upper and lower limits shaded in gray, calculated using $v = 0.15 \pm 0.05$ m s^{-1}. The *y* axis coordinate system for top right plot changes from a function of latitude from 16°S to 23°S to a function of longitude from 42°W to 44°W and the two regions are separated by a black straight line. (CF: Cabo Frio; CST: Cabo de São Tomé; V: Vitória; RD: Rio Doce; CA: Caravelas; CSM: Cabo de Santa Marta; TO: Torres; RG: Rio Grande.)

[80] The total upwelling transports for both Cabo Frio and Cabo de Santa Marta regions are mainly generated by wind-driven coastal upwelling which has a nearly uniform distribution. This upwelling, primarily wind-driven, is then modified first by horizontal shear gradients and second by changes in coastline curvature, which are both highly variable in space, and, in general, colocated. Topographically driven vertical motions are relevant upstream of coastal capes, acting against the wind-driven coastal upwelling and therefore reducing the total upwelling transport, and are also relevant downstream of capes, when all three mechanisms add up to create strong upwelling favorable sites along the coast.

[81] Comparisons between SST and upwelling transports reveal a good agreement, where local minima of temperature

are found slightly downstream of upwelling peaks, driven mainly by flow-topography interactions, while larger scale variability seems to be related to wind-driven mechanisms. Agreements between upwelling peaks due to topographic upwelling and SST are especially clear south of Rio Doce to the southern end of the Cabo Frio region, and south of Cabo de Santa Marta. Particular exceptions to that are found in two regions: between Rio Doce and Caravelas in the Cabo Frio region, and in the vicinity of Rio Grande in the Cabo de Santa Marta region.

[82] The region between Rio Doce and Caravelas has a very wide continental shelf, reaching up to 240 km, with the presence of complex bathymetry and a large coral reef system, the Abrolhos Bank. Two different mechanisms in this region could possibly affect the SST and cause the anomalous warm SST: first, the large extension of the shelf could possibly make the upwelling source water further away from the coast, and therefore it would take a longer time to reach the inner shelf, where most of the upwelling occurs due to Ekman transport. Second, the complex bathymetry, width of the shelf, and presence of coral reefs may considerably increase frictional effects that could damp the formation of the upwelling jet. The anomalous warm temperatures in the vicinity of Rio Grande cannot be explained by the upwelling transports from our model results, and it could possibly be due to the influence of the Patos Lagoon in the coastal ocean (Figure 4). The lagoon is very large, nearly 250 km long by 40 km wide, and since it is also very shallow with a mean depth of nearly 5 m, it gets significantly warmer from incoming solar radiation than the coastal ocean, potentially influencing the adjacent ocean surface waters.

[83] The degree to which a coastal upwelling jet separates from the coast due to perturbations in topography was studied by *Castelão and Barth* [2006a]. Based on a series of numerical simulations with idealized topography and real stratification, the authors found that maximum separation occurs with increasing Rossby number (*Ro*) and a Burger number (*Bu*) close to 1. A jet separation criterion was established based on *Castelão and Barth* [2006a], where the *Ro* was calculated from $Ro = \frac{v}{f\lambda_i}$ and $Bu = \frac{\lambda_i^2}{R^2}$ (Figure 8). In the Cabo Frio region, *Ro* shows very small change through the domain, from 0.13 ± 0.05 in the southern end to 0.2 ± 0.07 in the northern border. *Bu* has values close to zero in most of the domain, with the exception of four peaks: 0.23 at Caravelas, 0.1 at Rio Doce, 0.33 at Cabo de São Tomé, and 0.95 at Cabo Frio. In Cabo de Santa Marta, *Ro* numbers are small, around 0.1 with insignificant deviations from that within the study region. The *Bu* is also very small, near zero everywhere except for a peak at Cabo de Santa Marta reaching 0.08. The values found suggest that a jet separation is not likely to occur at Cabo de Santa Marta, however *Bu* close to one at Cabo Frio suggests that this is a preferred place for jet separation to occur. The analytical model used in this paper breaks down southward of Cabo Frio, where the upwelling jet is likely to separate off the coast according to the criteria based on *Castelão and Barth* [2006a]. Observational evidence of the jet separation does not currently exist.

[84] It is important to notice that the analytical model used in this paper assumes a steady state, and that the total upwelling transport is composed of simply a linear combination of the mechanisms studied (coastal upwelling, Ekman pumping, changes in horizontal shear, and coastline curvature), neglecting possible nonlinear interactions between them, time dependence, as well as any other mechanisms. Examples of other mechanisms not present in this model that have been shown to affect upwelling in the region of Cabo Frio include: feedbacks between sea breeze and coastal upwelling [*Franchito et al*., 1999], and coupling between SST, SST gradients, and wind stress curl [*Castelão*, 2012], and in the region of Cabo de Santa Marta, changes in the continental shelf width [*Campos et al*., 2013]. In the South Brazil Bight, interactions between the Brazil current and topography [*Palma and Matano*, 1989; *Matano et al*., 1986], and instabilities [*Campos et al*., 1995, 2000] may also be important.

[85] Our estimates of vertical transport due to flow-topography interactions, $W_{topography} = W_{tshear} + W_{tradius}$, is the sum of two distinct modes of the flow. One mode is that the coastal jet's offshore boundary remains straight and at a fixed distance from the mean position of the coastline, and that the jet changes its width, and the flow is "squeezed" (W_{tshear}). Another mode is that the coastal jet follows the coastline and the jet width is fixed ($W_{tradius}$). In the real ocean however, bottom topography and continuous stratification bring further complexity to the flow, and the contribution of the two modes may not necessarily be weighted equally. It is important to keep in mind that our estimates are in the upper limits of both mechanisms and those assumptions were necessary to make progress using analytical solutions. In fact the contribution of the flow-topography interactions to the upwelling transport could be better modeled by: $W_{topography} = \sigma * W_{tshear} + (1 - \sigma) * W_{tradius}$, where σ varies between 0 and 1, and numerical simulations could aid to find σ under different scenarios.

[86] Another important assumption used in the calculations of upwelling due to flow-topography interactions is the linear cross-shelf velocity profile of the coastal jet. This seems like a first natural choice for an analytical problem approximating a jet sheared by lateral friction, however the shape of the upwelling jet could in fact be a different one in the real ocean. This specific choice could possibly be underestimating the shear, when compared to other velocity profiles, such as a quadratic one for example. In order to validate the assumption for the velocity profile chosen, in situ measurements should be done over the region with proper spatial and temporal resolution, data that are not currently available.

[87] Finally, the choice of a two-layer model and the desire to obtain an analytical solution led to the necessity of making the assumptions given by equations (10) and (11). Previous analytical and numerical results from two-layer upwelling dynamics [e.g., *Crépon and Richez*, 1984; *Crépon et al*., 1961] show similar baroclinic behavior, where spatial variability in atmospheric forcing or coastline disturbances (e.g., capes) can generate a current flowing in the direction of the wind in the surface layer, and opposite to the wind in the bottom layer. This is a response due to the generation of internal Kelvin waves that arise under these conditions [e.g., *Allen*, 1975, 1976].

[88] In fact, *Crépon and Richez* [1984] and *Crépon et al*. [1961] show that the baroclinic component of the layer's velocities is related by:

$$v_2 = -v_1 \frac{h_1}{h_2} \quad (29)$$

which, in the case of a two-layer approximation, where $h_1 \approx h_2$, supports *Johnson et al*.'s [1980] assumptions.

[89] Departures from vertical velocity estimates in the two-layer model could arise due to the position of the pycnocline relative to the total water depth (or ratio of layer thicknesses). Observations from oceanographic cruises near Cabo Frio and Cabo de Santa Marta show that during summer time the pycnocline is positioned in between 20 and 30 m deep [*Miranda*, 2008; *Matsuura*, 1996; *Valentin et al*., 2002; *Möller et al*., 2009; *Campos et al*., 2013]. This would modify our estimates of vertical velocities, reducing them by $(1-h_1/h_2) \times 100\%$ which would effectively lead to a 25–60% slower upwelling, assuming again a constant flat-bottom topography of 70 m deep, as used in our analysis.

[90] Despite the simplicity of the analytical model, and our highly idealized assumptions, results in general agree well with the variability of observed sea surface temperature along the coast. Wind-driven upwelling mechanisms solely could not explain the observed SST along the coast, showing that the capes and coastal features have a fundamental role in the SST variability and upwelling velocities along the coast for both regions of Cabo Frio and Cabo de Santa Marta, Brazil. Results also strongly suggest that on larger scales, the SST variability along the coast is mainly controlled by wind-driven upwelling, while upwelling due to flow-topography interaction is responsible for the smaller scale SST variability.

6. Summary and Conclusions

[91] In this paper, we used an analytical, two-layer, steady, wind-driven model, and wind stress data from the QuikSCAT satellite to investigate the contributions of Ekman transport, Ekman pumping, coastline curvature, and horizontal shear due to coastline irregularities, to the total vertical transports in the major upwelling systems of Brazil, the regions of Cabo Frio and Cabo de Santa Marta. Both wind-driven and topographically driven upwellings are fundamental to describe the variability of SST and vertical transport structure along the coast. Away from coastline irregularities, wind-driven upwelling dominates. However, in the vicinity of capes and coastal features, topographically driven upwelling plays a significant role, and its transports vary from 43% to 94% of wind-driven upwelling, depending on how abrupt the coastline disturbances are. Results show that the upwelling system at Cabo Frio has vertical transports about twice as large as in the Cabo de Santa Marta region, because both topographically driven and wind-driven mechanisms are stronger in the Cabo Frio region.

[92] Using satellite remote sensing, it was possible to detect oscillations in SST along the coast, with warmer peaks upstream of capes and colder peaks downstream of capes, corresponding to the vertical transport variability predicted by the two-layer model. It also revealed the importance of including topographically driven upwelling in the total vertical transports to explain SST patterns along the coast, which could not be done by only using the wind-driven mechanisms. Wind-driven and topographically driven upwelling act on different spatial scales: large-scale SST variability is controlled mainly by wind-driven upwelling, while smaller scale SST variability is controlled by upwelling driven by flow-topography interaction.

[93] Ocean observing technologies available today, such as high-frequency, land-based coastal radars, underwater gliders, moorings, etc., as well as fully nonlinear primitive equation numerical models should be used in future research in order to fully understand the complex upwelling dynamics of the Brazilian coast. Future studies of upwelling dynamics in these regions should address time dependence, wind relaxations and reversals, the role of barotropic and baroclinic waves and tides, as well as the influence of the western boundary Brazil current.

[94] **Acknowledgments.** This work was primarily supported by a Brazil-U.S. CAPES/Fulbright scholarship to Piero Luigi Fernandes Mazzini. Additional support was provided by the U.S. National Science Foundation grants OCE 0851486 and OCE 0961999.

References

Allard, P. (1955), Anomalies dans le temperature de leau de la mer observees au Cabo Frio au Bresil, *Bull. Inf. Comite Cent. Oceanogr. Etud. Cotes*, *7*(2), 58–63.

Allen, J. S. (1975), Coastal trapped waves in a stratified ocean, *J. Phys. Oceanogr.*, *5*, 300–325.

Allen, J. S. (1976), Some aspects of the forced wave response of stratified coastal regions, *J. Phys. Oceanogr.*, *6*(1), 113–119.

Arthur, R. S. (1965), On the calculation of vertical motion in eastern boundary currents from determinations of horizontal motion, *J. Geophys. Res.*, *70*(12), 2799–2803.

Campos, E. J. D., J. Goncalves, and Y. Ikeda (1995), Water mass characteristics and geostrophic circulation in the South Brazil Bight: Summer of 1991, *J. Geophys. Res.*, *100*(C9), 18,537–18,550.

Campos, E. J. D., J. A. Lorenzzetti, M. R. Stevenson, J. L. Stech and R. B. Souza (1996), Penetration of waters from the Brazil-Malvinas Confluence Region along the South American continental shelf up to 23°8S, *Acad. Bras. Ciënc.*, *68*(1), 4958.

Campos, E. J. D., C. A. D. Lentini, J. L. Miller and A. R. Piola (1999), Interannual variability of the sea surface temperature in the South Brazil Bight, *Geophys. Res. Lett.*, *26*(14), 2061–2064.

Campos, E. J. D., D. Velhote, and I. da Silveira (2000), Shelf break upwelling driven by Brazil Current cyclonic meanders, *Geophys. Res. Lett.*, *27*(6), 751–754.

Campos, P. C., O. O. Moller, Jr., A. R. Piola, and E. D. Palma (2013), Seasonal variability and coastal upwelling near Cape Santa Marta (Brazil), *J. Geophys. Res.*, *118*, 1420–1433, doi:10.1002/jgrc.20131.

Capet, X. J., P. Marchesiello and J. C. McWilliams (2004), Upwelling response to coastal wind profiles, *Geophys. Res. Lett.*, *31*, L13311, doi:10.1029/2004GL020123.

Castelão, R. M., and J. A. Barth, (2006a), The relative importance of wind strength and along-shelf bathymetric variations on the separation of a coastal upwelling jet, *J. Phys. Oceanogr.*, *36*, 412–425.

Castelão, R. M., and J. A. Barth (2006b), Upwelling around Cabo Frio, Brazil: The importance of wind stress curl, *Geophys. Res. Lett.*, *33*, L03602, doi:10.1029/2005GL025182.

Castelão, R. M. (2012), Sea surface temperature and wind stress curl variability near a cape, *J. Phys. Oceanogr.*, *42*, 2073–2087.

Castro, B. M., and L. B. Miranda, (1998), Physical oceanography of the western Atlantic continental shelf located between 4 N and 34 S coastal segment (4, W), *Sea*, *11*, 209–251.

Chelton, D. B., and M. H. Freilich (2005), Scatterometer-based assessment of 10-m wind analyses from the operational ECMWF and NCEP numerical weather prediction models, *Mon. Wea. Rev.*, *133*, 409–429.

Chelton, D. B., M. F. Schlax, M. H. Freilich, and R. F. Milliff (2004), Satellite measurements reveal persistent small-scale features in ocean winds, *Science*, *303*(5660), 978–983.

Crépon, M., and C. Richez (1982), Transient upwelling generated by two-dimensional atmospheric forcing and variability in the coastline, *J. Phys. Oceanogr.*, *12*, 1437–1457.

Crépon, M., C. Richez, and M. Chartier (1984), Effects of coastline geometry on upwellings, *J. Phys. Oceanogr.*, *14*, 1365–1382.

Emílsson, I. (1961), The shelf and coastal waters off southern Brazil, *Bol. Inst. Oceanogr.*, *11*(2), 101–112.

Ekman, V. W. (1905), On the influence of the Earths rotation on ocean currents, *Arch. Math. Astron. Fys.*, *2*(11), 1–53.

Figueroa, D., and C. Moffat (2000), On the influence of topography in the induction of coastal upwelling along the Chilean Coast, *Geophys. Res. Lett.*, *27*(23), 3905–3908.

Franchito, S., V. Rao, J. Stech, and J. Lorenzzetti (1998), The effect of coastal upwelling on the sea-breeze circulation at Cabo Frio, Brazil: A numerical experiment, *Ann. Geophys.*, *16*, 866–881.

Freilich, M. H., and R. S. Dunbar (1999), The accuracy of the NSCAT-1 vector winds: Comparisons with NDBC buoys, *J. Geophys. Res.*, *104*(11), 231–246.

Freilich, M. H., D. G. Long, and M. W. Spencer (1994), SeaWinds: A scanning scatterometer for ADEOS IIScience overview, in Proceedings of the International Geoscience and Remote Sensing Symposium, pp. 960–963, IEEE, Pasadena, Calif.

Ikeda, Y., L. B. Miranda, and I. C. Miniussi (1974), Observations on stages of upwelling in the region of Cabo Frio (Brazil) as conducted by continuous surface temperature and salinity measurements, *Bol. Inst. Oceanogr.*, *23*, 3346.

Johnson, D. R., T. Fonseca, and H. Sievers (1980), Upwelling in the Humboldt coastal current near Valparaíso, Chile, *J. Mar. Res.*, *38*(1), 1–16.

Lentini, C. A. D., G. G. Podestá, E. J. D. Campos, and D. B. Olson (2001), Sea surface temperature anomalies on the Western South Atlantic from 1982 to 1994, *Cont. Shelf Res.*, *21*(1), 89–112.

Lima, I. D., C. E. Garcia, and O. O. Möller (1996), Ocean surface processes on the southern Brazilian shelf: Characterization and seasonal variability, *Cont. Shelf Res.*, *16*(10), 1307–1317.

Magliocca, A., L. B. Miranda, and S. R. Signorini (1979), Physical and chemical aspects of transient stages of the upwelling at southwest of Cabo Frio (Lat.23°S–Long.42°W), *Bol. Inst. Oceanogr.*, *28*(2), 3746.

Matano, R. P., E. D. Palma, and A. R. Piola (2010), The influence of the Brazil and Malvinas Currents on the southwestern Atlantic shelf circulation, *Ocean Sci. Discuss.*, *7*(2), 837–871.

Matsuura, Y. (1986), Contribuição ao estudo da estrutura oceanográfica da região sudeste entre Cabo Frio (RJ) e Cabo de Santa Marta Grande (SC), *Ciênc. Cult.*, *38*(8), 1439–1450.

Matsuura, Y. (1996), A probable cause of recruitment failure of Brazilian Sardine (Sardinella aurita) population during the 1974/75 spawning season, *S. Afr. J. Mar. Sci.*, *17*, 29–35.

Matsuura, Y. (1998), Brazilian Sardine (Sardinella brasiliensis) spawning in the southeast bight over the period 1976/93, *Rev. Brasil. Oceanogr.*, *46*, 33–43.

Miranda, L. B. (1982), Análise de massas de água da plataforma continental e da região oceânica adjacente: Cabo de Sâo Tomé (RJ) e Ilha de São Sebastião (SP), ''Livre Docência'' thesis, 123 pp., Univ. de São Paulo, São Paulo, Brazil.

Möller, O. O., Jr., A. R. Piola, A. C. Freitas, and E. J. D. Campos (2008), The effects of river discharge and seasonal winds on the shelf off southeastern South America, *Cont. Shelf Res.*, *28*(13), 1607–1624.

Palma, E. D., and R. P. Matano (2009), Disentangling the upwelling mechanisms of the South Brazil Bight, *Cont. Shelf Res.*, *29*(11–12), 1525–1534.

Pereira, C. S. (1989), Seasonal variability in the coastal circulation on the Brazilian continental shelf (29°S–35°S), *Cont. Shelf Res.*, *9*(3), 285–299.

Piola, A. R., E. J. D. Campos, O. O. Möller, Jr., M. Charo, and C. Martinez (2000), Subtropical Shelf Front off eastern South America, *J. Geophys. Res.*, *105*(C3), 6565–6578.

Piola, A. R., R. P. Matano, E. D. Palma, O. O. Möller, Jr., and E. J. D. Campos (2005), The influence of the Plata River discharge on the western South Atlantic shelf, *Geophys. Res. Lett.*, *32*, L01603, doi:10.1029/2004GL021638.

Piola, A. R., O. O. Möller, Jr., R. A. Guerrero, and E. J. D. Campos (2008), Variability of the Subtropical Shelf front off eastern South America: Winter 2003 and summer 2004, *Cont. Shelf Res.*, *28*, 1639–1648.

Risien, C. M., and D. B. Chelton (2008), A global climatology of surface wind and wind stress fields from eight years of QuikSCAT scatterometer data, *J. Phys. Oceanogr.*, *38*, 2379–2413.

Rodrigues, R. R., and J. A. Lorenzzetti (2001), A numerical study of the effects of bottom topography and coastline geometry on the Southeast Brazilian coastal upwelling, *Cont. Shelf Res.*, *21*(4), 371–394.

Soares, I. D., and O. O. Möller Jr. (2001), Low-frequency currents and water mass spatial distribution on the southern Brazilian shelf, *Cont. Shelf Res.*, *21*(16), 1785–1814.

Souza, R. B., and I. S. Robinson (2004), Lagrangian and satellite observations of the Brazilian Coastal Current, *Cont. Shelf Res.*, *24*(2), 241–262.

Stark, J. D., C. J. Donlon, M. J. Martin, and M. E. McCulloch (2007), OSTIA: An operational, high resolution, real time, global sea surface temperature analysis system, in Oceans '07 IEEE Aberdeen, Conference Proceedings. Marine Challenges: Coastline to Deep Sea, IEEE, Aberdeen, Scotland.

Stech, J. L., and J. A. Lorenzzetti (1992), The response of the South Brazil Bight to the passage of wintertime cold fronts, *J. Geophys. Res.*, *97*(6), 9507–9520.

Valentin, J. L., D. L. Andre, and S. A. Jacob (1987), Hydrobiology in the Cabo Frio (Brazil) upwelling: Two-dimensional structure and variability during a wind cycle, *Cont. Shelf Res.*, *7*(1), 77–88.

Zavialov, P., O. O. Möller, Jr., and E. Campos (2002), First direct measurements of currents on the continental shelf of Southern Brazil, *Cont. Shelf Res.*, *22*, 1975–1986.